energies

MDPI

Article

Experimental and Finite Element-Based Investigation on Lateral Behaviors of a Novel Hybrid Monopile

Jeongsoo Kim [1,*], Yeon-Ju Jeong [2], Joonsang Park [3], Ju-Hyung Lee [4], Taeyoung Kwak [4] and Jae-Hyun Kim [5]

[1] Department of Future and Smart Construction Research, Korea Institute of Civil Engineering and Building Technology, Goyang 10223, Republic of Korea
[2] Department of Structural Engineering Research, Korea Institute of Civil Engineering and Building Technology, Goyang 10223, Republic of Korea
[3] Section of Geohazards and Dynamics, Norwegian Geotechnical Institute, 3930 Oslo, Norway
[4] Department of Geotechnical Engineering Research, Korea Institute of Civil Engineering and Building Technology, Goyang 10223, Republic of Korea
[5] Department of Civil Engineering, Kangwon National University, Chuncheon 24341, Republic of Korea
* Correspondence: jeongsookim@kict.re.kr; Tel.: +82-31-910-0093

Abstract: A monopile is the most conventional structure foundation for offshore wind turbines (OWTs) in the world. However, the Korean offshore wind industry has mostly been using the jacket type of foundation. The main reason for the current situation in Korea is that most of the marine soil consists of weak layers of sand and clay. Thus, the monopile foundation depth has to be deep enough to satisfy the intended serviceability design requirement of the monopile and the rotation limit at the seabed; a conventional monopile design concept alone might be insufficient in Korean offshore conditions, or otherwise could be very expensive, e.g., resulting in a rock socket installation at the tip of the monopile. The main objective of this paper is to introduce a novel hybrid monopile that is composed of a monopile and a supplemental support with three buckets, followed by assessing the lateral resistance of the hybrid system through physical experiments and finite element (FE) simulations. Namely, 1/64.5 small-scaled monopile and hybrid physical models with a monopile diameter of 7 m for a 5.5 MW OWT were loaded monotonically. The results show that the hybrid monopile improves the lateral bearing capacity regarding the initial lateral stiffness and ultimate load. The FE analyses of the corresponding physical models were also implemented to support the results from the physical model test. The numerical results, such as the structural member forces and soil deformation, were analyzed in detail. Additionally, a case study using FE analysis was conducted for the 5.5 MW OWT hybrid monopile support installed in a representative Korean weak soil area. The results show that the hybrid monopile foundation has a larger lateral resistance and stiffness than the monopile.

Keywords: hybrid monopile; supplemental support; physical modelling; finite element analysis; lateral resistance

Citation: Kim, J.; Jeong, Y.-J.; Park, J.; Lee, J.-H.; Kwak, T.; Kim, J.-H. Experimental and Finite Element-Based Investigation on Lateral Behaviors of a Novel Hybrid Monopile. *Energies* **2022**, *15*, 9095. https://doi.org/10.3390/en15239095

Academic Editor: José António Correia

Received: 30 October 2022
Accepted: 21 November 2022
Published: 30 November 2022

1. Introduction

As offshore wind energy has become more price competitive than before, Europe and many countries have made significant efforts during recent decades to increase wind energy's contribution to their own electricity supply. On the other hand, the Korean offshore wind industry is still in its early stages of development, and only recently has made a commitment to increase its offshore wind capacity to 12 GW by 2030. Unlike the European offshore seabed in which predominantly sandy soils are distributed, most of the Korean seabed consists of weak soil both widely and deeply, except for the coastal area near Jeju Island. Such soil characteristics are not appropriate to construct monopile foundations for OWTs. Therefore, the jacket type foundation has been preferred in Korea, although it is rather expensive and time-consuming to construct. However, through the recent extensive

use of monopiles and the accumulation of technical experience, monopile technologies with optimized design and manufacturing in Korea have developed quickly and become available even in water up to around 60 m deep [1]. Furthermore, attempts to develop the domestic production capacity for XL monopiles (>7 m diameters) have also been ongoing in Korea.

As the OWT capacity has increased to satisfy economic feasibility, and in turn the average water depth of farms increased from 2009 to 2016, offshore wind farms are hence installed far from the nearest shorelines [2], which in turn has increased the construction costs. To support the new generation of OWTs which have a more electric power capacity, conventional offshore fixed monopiles have to be rammed deeper into the seabed and enlarged to resist extreme environmental forces [2,3]. As a result, new foundation concepts have been discussed and studied in the wind energy community [2,4–15]. Several new concepts in previous studies have been reported to reduce the weight of large monopiles [7] and improve the serviceability of OWTs by constraining a lateral displacement at the pile head [4–6,8–14], e.g., monopiles with footing such as circular plates, gravel wheels, and suction mats at the pile head to decrease the rotational displacement at the seabed. Such a concept can reduce the pile penetration depth and the cost of a foundation installation. These advantages prompted the first hybrid monopile installation of an offshore wind farm at the Putian Pinghai Phase II site in China [16]. The hybrid monopile had a large suction bucket as a supplemental support, and its performances were verified by centrifuge tests of small-scaled models and FE analyses [17]. After that, in 2022, large monopiles with collared supports were placed at the Kaskasi offshore wind farm in Germany [18,19]. Before the installation, the collared support was designed by parametric structural analyses to be applied to a monopile for a 5 MW OWT [20]. Moreover, in addition to the collar, similar shapes for the supplemental support were tested to analyze the load transfer mechanism of the collared monopile using small-scaled models with various sizes of supplemental support under 1 g condition systems [5,21].

The current paper proposes a novel concept of hybrid OWT foundations by the combining of a large monopile and three buckets. Figure 1 shows the scheme of the structure. The monopile is the same as the conventional one but has shear keys to apply grouted joints between the monopile and the supplemental support attached to the outer surface of the monopile. Considering the satisfaction with the serviceability design requirement of the monopile, more buckets can make the hybrid system more stable and rigid. However, as the number of buckets increases, tilting inevitably occurs during the supplemental support installation, making it hard to control. For this reason, the tri-bucket is adapted as the supplemental support to balance the bearing capacity, stability, and installation of the hybrid monopile. Meanwhile, the potential dimensions for the XL monopile and the supplemental support are indicated in Figure 1. The diameter of the monopile was selected as 7 m, which is the same as that of Korean research projects on OWT monopiles [1,22]. The thickness of the monopile was designed based on DNV-GL codes [23] to be within the ratio of the diameter to the thickness of 80~90; the objective of the ratio requirement is to prevent the monopile from buckling, and the ratio is 87.5, as shown in Figure 1. The dimensions of the supplemental support were also determined considering the size of the monopile by roughly estimating the soil bearing capacities of the Korean offshore sites for offshore wind farms.

The supplemental support consists of three suction buckets, which are maintained in 120 degrees, and a main cylindrical sleeve of which the inner surface has shear keys. For the supplemental support, the buckets are connected to the sleeve by truss members to distribute external forces transmitted from the monopile. Although the proposed hybrid monopile is more complex than the conventional monopile with respect to the design due to the connection members, the proposed monopile can be proper to the area which has widely distributed weak and ununiform soil as well deep water like the Korean seabed. The hybrid monopile has the following installation procedure, as shown in Figure 2. First, the supplemental support is placed at a target area and is penetrated into the soil layers by

suction. For the monopile installation process, the supplemental support can be a role as a pre-piling template, which guides the monopile driving. After the monopile is then inserted in the sleeve and penetrated partially by hammering or vibration, the space between the monopile and the sleeve is filled with high strength grout. When the monopile is completely connected with the supplemental support, the monopile is driven to the target depth, with tilting correction by the suction pressure controlling of the supplemental support.

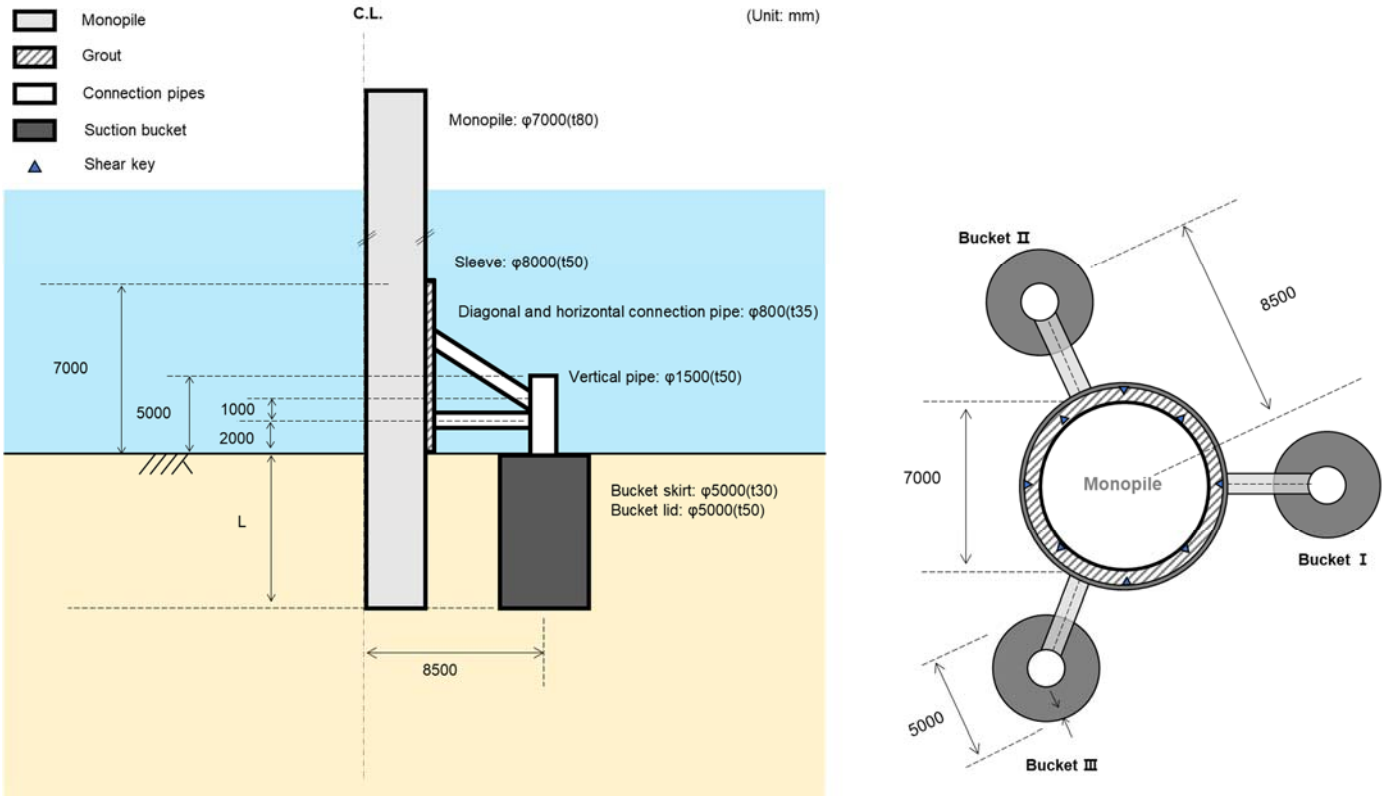

Figure 1. Scheme of hybrid foundation combining with a monopile and tri-buckets: (**a**) side view; (**b**) top view, where C.L.: centerline of the hybrid monopile, L: embedding length of the monopile, φ: diameter of the cross-section of structural members.

In this paper, the proposed new type of hybrid monopile was analyzed by both the experiment and finite element (FE) method for small-scaled models to investigate the lateral behaviors of the proposed hybrid monopile compared with those of the conventional monopile. Additionally, to compensate the small-scaled tests, several FE analyses of a 5.5 MW OWT hybrid monopile substructure with the monopile diameter of 7 m were implemented.

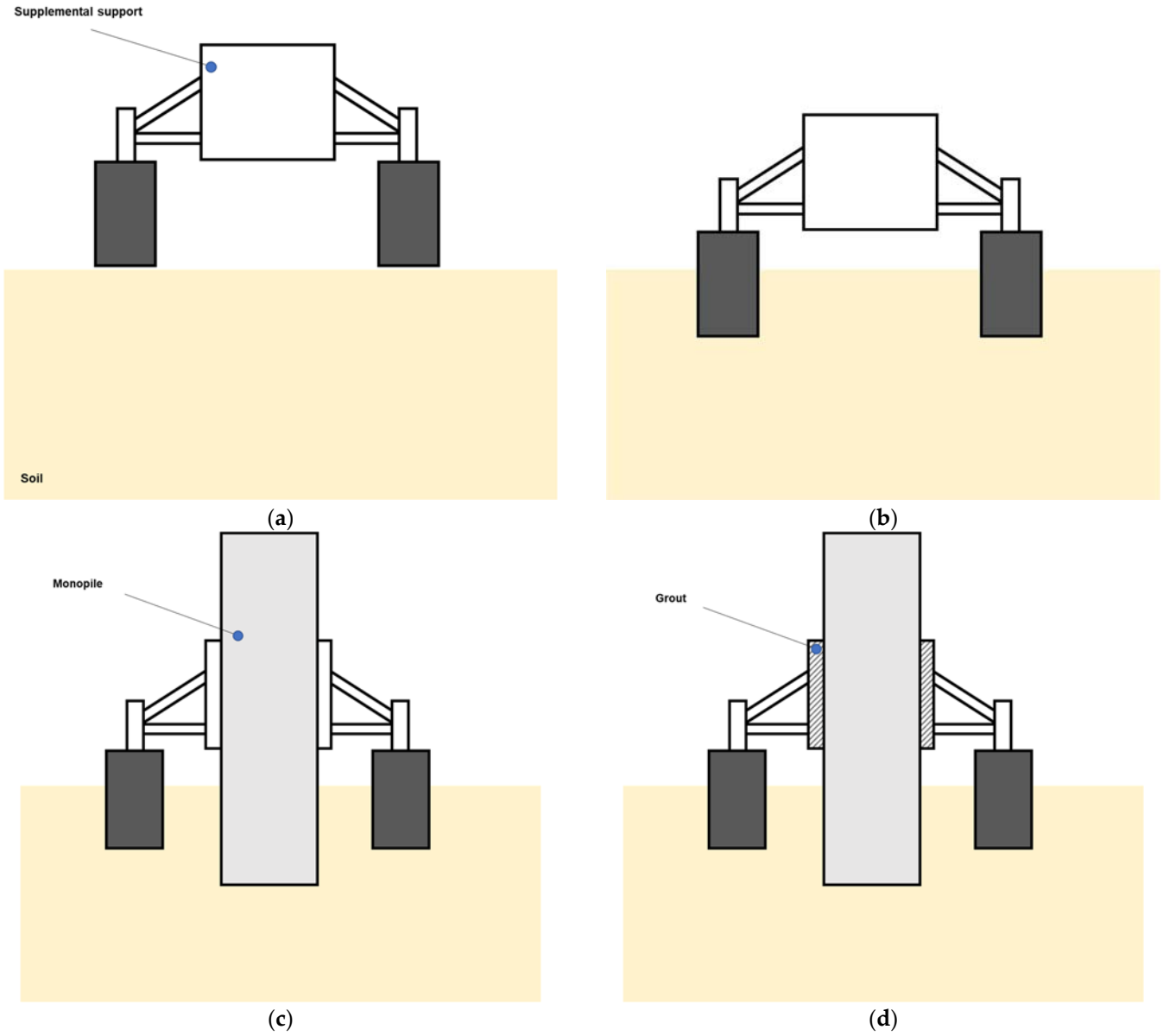

Figure 2. Hybrid monopile installation procedure (**a**) supplemental support placement; (**b**) penetration by suction; (**c**) monopile installation; (**d**) grouting and penetration.

2. Physical Tests and FE Model of Hybrid Monopile

2.1. Pysical Model Test

2.1.1. Tests Models

Many loading tests and soil foundation set-up in laboratory tests for monopiles have been dealt in previous research [2,4,5,8,17,20]. Depending on the resources and equipment available, the test setups can be totally different for monopile loading tests even with the same objectives. Nevertheless, for all small-scaled models, similar rules for the material properties or the geometries of real structures have to be maintained.

In this study, several physical model tests were conducted to investigate changes in the lateral behavior of each type of monopile. As shown in Figure 3, two types of physical models with a scale factor of 1:64.5 for a 5.5 MW OWT substructure were fabricated to represent the proposed hybrid monopile and the conventional one; the weight of each model was 7.05 kg and 9.35 kg, respectively. A model for the conventional is a steel pipe with a diameter of 109.62 mm, while the other not only includes the pipe but also a

supplemental support that consists of three buckets with a diameter 77.5 mm and connects to the pipe with bolts. Other specific dimensions appear in Table 1.

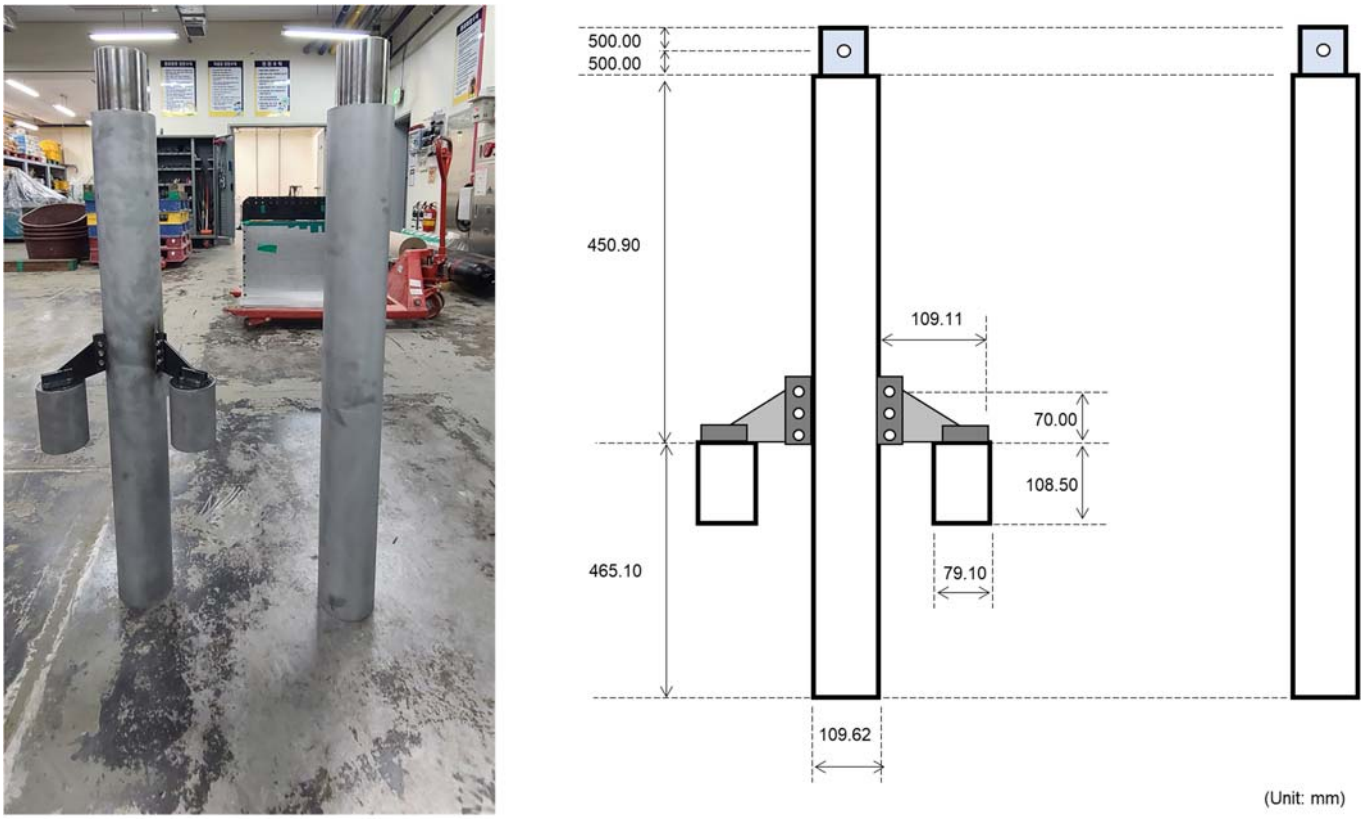

(**a**) (**b**)

Figure 3. Physical test models of hybrid and conventional monopiles: (**a**) small-scaled test models; (**b**) dimensions of small-scaled tests models.

Table 1. Dimensions of the proposed hybrid monopile for physical test model.

Hybrid Monopile Component	Geometry	Dimension (mm)
Monopile *	Outer diameter	109.62
	Thickness	1.62
	Penetration depth	465.10
	Loading point (distance from soil surface)	516.80
Supplemental support	Outer diameter	79.10
	Thickness	1.62
	Penetration depth	108.50
	Distance between monopile and supplemental support	38.76

* The physical test model for the conventional monopile has the same dimensions with those of the proposed hybrid monopile.

To transfer a transverse load to the models without unintended loads, the connection pipe on the top of each model was bonded. Before the models were penetrated into the soil foundation, the surfaces of them were sand-blasted to increase the surface roughness and the average roughness was measured as 4.82 μm.

2.1.2. Foundation Soil Set-Up and Measurement System

In order to measure the lateral resistance and displacement of the model, the test model included soil mold, a load application device, and data acquisition devices such as a load cell and laser sensor.

For the laboratory test, the soil sample was taken from Gunsan Saemangeum (GS) which is one of the candidate sites of the offshore wind farm project in South Korea. Before setting up the soil foundation, several soil test such as the sieve test and triaxial compression test were conducted to estimate the soil properties. The soil was classified as silty sand according to USCS (SM, 47% of soil passing No. 200 sieve) and the other soil fundamental properties as shown in Table 2; the permeability coefficient were not measured, but the value was referred from another related study where the soil fundamental parameters for the same area were not only similar to those of this study but also the permeability coefficient was measured. Additionally, the soil strength parameters were measured by a triaxial compression test under a consolidated drained (CD) condition. For 100~400 kPa confining pressure, the internal friction angles of the soil samples were estimated. The peak values were varied from 35.8° to 39.4° with a confining stress and relative density while the residual was estimated to be 35.5°.

Table 2. Fundamental parameters of GS soil sample.

Parameter	Value
The maximum dry density ($\rho_{d,max}$, kg/m^3)	1650
The minimum dry density ($\rho_{d,min}$, kg/m^3)	1200
Specific gravity (G_s)	2.67
Uniformity coefficient (C_u)	2.11
Mean effective grain size (D_{50}, mm)	0.08
Permeability coefficient (k, m/s)	1.5~2.0 $\times 10^{-6}$
Void ratio	0.76~0.90
Peak internal friction angle (ϕ'_p, °)	35.8~39.4
Residual internal friction angle (ϕ'_r, °)	35.5

For setting up the soil foundation, a cylindrical steel mold with an inner diameter of 900 mm and a height of 700 mm was used, as shown in Figure 4. The soil foundations were generated by stacking up 11 layers to a height of 550 mm into the mold; each layer has a height of 50 mm and was compressed by dropping a 13.5 kg weight, referring to the standard proctor compaction test. After completing the soil foundation's set-up, water was slowly supplied to the soil to be saturated; the water level was kept at the height of 3 cm from the soil surface during the physical tests. The soil foundation condition for both the conventional and the hybrid monopiles are listed in Table 3; the relative density of each sandy soil foundation is similar to that of each other, so approximate soil behaviors could be expected.

(**a**) (**b**) (**c**)

Figure 4. Soil foundation setting: (**a**) soil sprinkle; (**b**) soil compaction; (**c**) soil foundation set-up.

To obtain the lateral behavior data of the models, a loading system including several apparatuses was used as shown in Figure 5a. The system consists of a loading frame, load cell, and laser sensor. The loading frame is fixed to the soil mold and can control its loading arm position, thereby changing the loading point, and the magnitude of the lateral loading can be control. A hinge type of clamp, which connects the loading arm to physical

models, was adopted to minimize the inevitably constraining rotations of physical models. The load cell and laser sensor were used to acquire the lateral load and displacement data, respectively. The load cell with a 10 kN load capacity was placed between the hinge clamp and the loading arm while the laser sensors were attached to the opposite side of the loading frame, as shown in Figure 5b. The lateral displacements of the models were acquired from the laser sensor, located at the top, and the rigid rotation of the model was calculated from the data of three laser sensors; the similarity ratio of geometry was applied.

Table 3. Fundamental properties of soil foundation for conventional and hybrid monopiles.

Case	Layer Thickness (mm)	Water Content (%)	Dry Density (kg/m^3)	Moist Density (kg/m^3)	Relative Density (%)
Monopile (T1)	550	19.0	1340	1600	38.3
Hybrid monopile (T2)	550	18.0	1350	1600	41.1

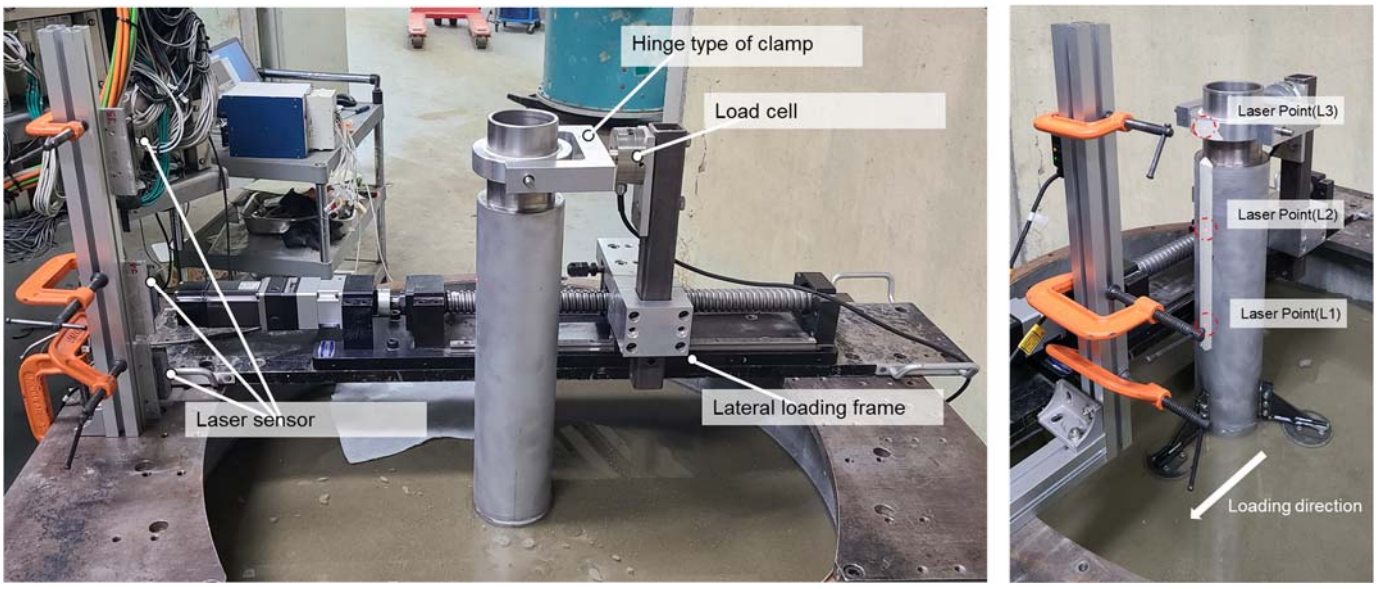

(**a**) (**b**)

Figure 5. Loading system: (**a**) main components; (**b**) laser senor measurement.

In Figure 5b, the notation L1, L2, and L3 indicate the laser sensor points. Each sensor was located from the soil surface as follows: 200 mm (L1), 360 mm (L2), and 510 mm (L3). Although L3 corresponds to the loading point, not the top of the monopile, the lateral displacement data from L3 were corrected, assuming the monopile shows a perfectly rigid rotation, to compare with the numerical results.

2.1.3. Test Condition and Procedure

For the conventional and the hybrid monopile models installed in cohesionless soil, both displacements of the structures and the soil resistance in the lateral direction were measured. The tests were designed to compare the lateral responses of the foundation types; thus, the test models were fabricated to be the same dimensions of each other for the diameter, penetration depth, and loading point location. Although the lateral behaviors of the hybrid monopile depend on the applied load directions, one lateral external force in the direction was applied, as shown in Figure 5b, to be the symmetric condition for the geometry and loading condition.

The test models were placed on the surface of the soil and were then penetrated into the soil with the compression load by the displacement control to the depth of 465.1 mm with the velocity of 0.5 mm/s; for your information, unlike explaining the installation

procedure of the hybrid monopile in Section 1, the hybrid model was connected with the supplemental support by bolts before the installation. After completing the installation of the models, the loading system and the data measurement devices were set to obtain the lateral responses of each model. A lateral displacement load was applied by the loading system with 0.1 mm/s until the rigid rotation of the model is until 6 degrees when the soil failure is observed.

2.2. FE Model Test

The FE models can help to understand the improvement mechanism of the proposed hybrid monopile more clearly and to analyze the results that were not measured in the physical tests. Finite element analyses were also conducted to supplement the physical tests, using the commercial finite element analysis program DIANA FEA, which is one of the powerful tools to solve the nonlinear problems of the structure and soil. For more details, refer to other publications on the FE method for solid and structural analysis [24]

2.2.1. Model Descriptions

Two half-symmetry models were built using shell and solid elements to reproduce the main structure, such as the monopile and the supplemental support, and the soil as well as the wall of the steel mold, and the models and discretization are shown in Figure 6. The models have the same dimensions with the physical test models and the bolt connections of the wing plate with the bucket or the monopile were simplified as a bond condition. The behaviors of the main structure and the GS sand were defined using a linear elastic model and a Mohr–Coulomb (MC) model, respectively. The MC plastic criteria can be written as:

$$\tau_f = c + \sigma_n \tan \phi' \quad (1)$$

where τ_f is the shear strength; c is the cohesion strength; σ_n is the normal stress on the failure surface; and ϕ' is the internal friction angle. The steel mold was considered as a rigid body; the elements for the steel mold were just introduced to prevent the artificial stress concentration of the soil due to the boundary conditions; and the contact interface between the steel mold and the sand were made to behave frictionless. The interface elements between the main structure and soil were also applied to transfer the compression only, not the tension. Although making the skin of the main structure rough, because the frictional resistance on the skin was rarely expected, the Coulomb friction model with the following parameters was adopted: the friction angle of 35.5°, the initial normal stiffness of 1×10^6 kN/m^3, and the initial normal stiffness of 10 kN/m^3.

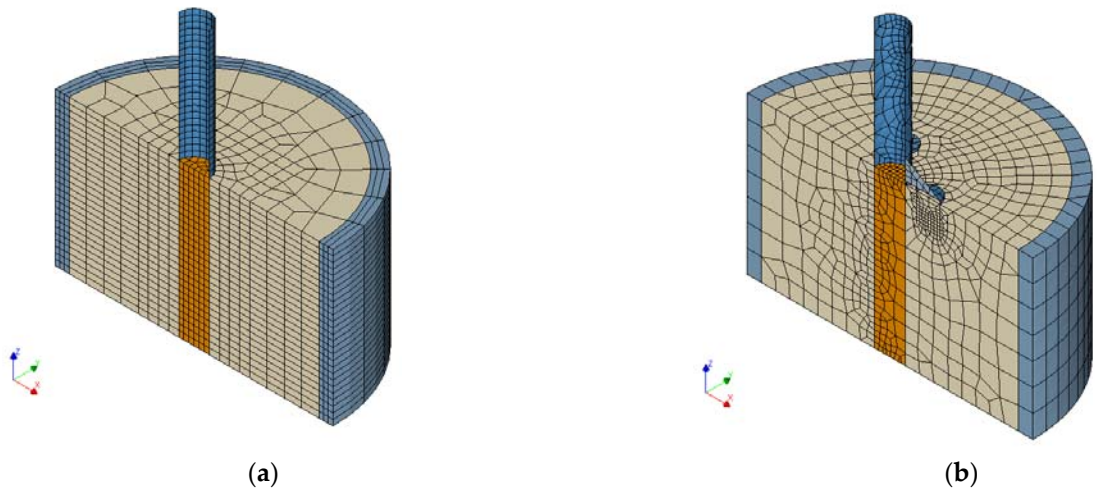

(**a**) (**b**)

Figure 6. Finite element models of physical test models: (**a**) monopile (**b**) hybrid monopile; where each color indicates mesh for a part; greyish blue: cylindrical steel mold, sorrel brown: soil foundation, yellowish orange: soil in and beneath monopile, and cool blue: monopile and supplemental support.

The mechanical parameters of steel were assigned as S355, including the elastic modulus of 200 GPa, the Poisson ratio of 0.3, and the unit weight of 78.65 kN/m^3; the submerged unit weight of the steel was applied to the part below the water level. In other hands, the soil mechanical and strength parameters were referred to Table 2, and the others such as the elastic modulus, dilatancy angle, and hardening parameters were inevitably assumed, as shown in Table 4. In particular of the soil elastic modulus, although the elastic modulus can be estimated using the results for triaxial compression tests, it was difficult to find the deformation parameter to reproduce the real behavior of the physical model due to the scale effect under a 1 g condition. When considering the relative density, void ratio, and confining stress level of Table 3, the soil elastic modulus was estimated to be 38.1 kPa [25]. However, in some preliminary FE simulations using the value for the physical tests, the FE models were not able to predict the lateral load–displacement relations similarly to those of the physical models; both a low initial stiffness and ultimate lateral resistance of the model were shown. For this reason, several inverse analyses were conducted to find the soil elastic modulus and hardening parameters predicting the load–displacement curve of the monopile test model properly.

Table 4. Mechanical and strength parameters of soil for numerical model for physical model test.

Parameter	Value
Submerged density (ρ, kg/m^3)	600
Elastic modulus (E, kPa)	3000 [1]
Poison's ratio (ν)	0.4
Porosity (n)	0.396
Cohesion (c, kPa)	0.1
Internal friction angle (ϕ', °)	35.5
Dilatancy angle (ψ', °)	20.5

[1] The value was estimated by fitting to the load–displacement curve.

The outer surface of the mold was constrained horizontally while the bottom of both the soil and the mold were constrained vertically. Additionally, in the y-direction in Figure 6, boundary conditions were applied considering the model symmetry. Note that the thickness of the wing plate on the symmetric plane was half for the hybrid monopile model. To prevent a stress concentration near the loading point, the displacements of the nodes on the edge at the top were constrained to be identically displaced in the load direction.

2.2.2. Construction Stage Analysis

The FE analyses were conducted in three stages: geostatic state analysis, physical model installation, and lateral loading. In the geostatic analysis, the soil elements were activated only and the initial horizontal effective stress of the elements was assumed to be 0.667 times of the vertical effective stress. After the structure elements were activated in the installation stage, the lateral displacement of 50 mm on the top end of the monopile was imposed for 16 steps.

3. Experimental and Numerical Results for the Small-Scaled Model

A lateral resistance of each foundation model was extracted from the displacement loading point at the top of the monopiles. For each foundation test, the experimental and numerical displacements were then compared and the soil and structure stress distributions were investigated to explain the behaviors of the physical models. Severe nonlinearity of numerical results due to low strength parameters and a concentrated contact area such as a monopile tip were observed. Therefore, stress singularities appeared at an abrupt geometry change or different material contact surface. For each step, a relative displacement norm less than 0.01, which is slightly less robust, was used as the convergence criteria to have converged results.

3.1. Monopile Test (T1)

Figure 7 shows the ultimate state of the physical model and lateral displacements by laser sensors as well as the lateral displacement numerically calculated. As the lateral displacement increased, the soil resistance measured by the load cell nonlinearly increased. Although the resistance was almost linear for the initial loading of T1, the stiffness decreased rapidly to be the yield; the peak resistance was estimated as 0.5 kN. According to the Vilalobos method [26] estimating the yield loading point of the soil foundations, T1 had the yield resistance of 0.4 kN.

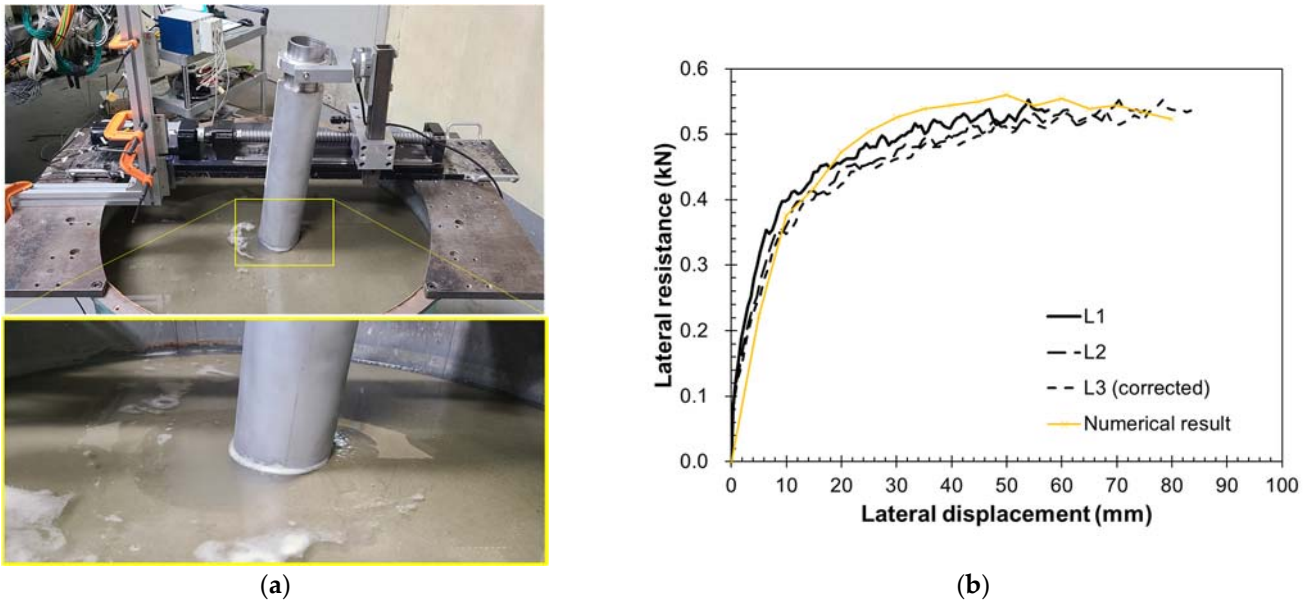

(**a**) (**b**)

Figure 7. Physical and FE-based test comparison for monopile: (**a**) surface subsidence after loading of physical test; (**b**) load–displacement curves from physical and FE models.

Though the numerical results were obtained by the inverse analysis of T1, both the slopes of the experimental and the numerical curves were similar to each other and showed good agreements until at 10 mm. However, the former shows a continuous hardening after the yield resistance while the latter shows a softening after the peak resistance of 0.56 kN at 50 mm.

Figure 8 shows the equivalent plastic strain changes to visualize the soil failure mechanism for the monopile. The failure area became wider and deeper as the top displacement increased. Plastic deformation occurred near the vicinity of the end tip at the initial installation. After applying the lateral load, the stresses of soil around the compression area of the monopile tip were concentrated, and the surface of the soil around the pile became plastic. As the lateral displacement of the monopile increased, the plastic area expanded to the steel mold so most of the soil in the compression direction failed, while the soil failure area around the monopile in the other side failed. However, unlike the physical test, the FE model cannot reproduce the soil subsidence of the soil surface in the opposite direction of the load.

3.2. Hybrid Monopile Test (T2)

Figure 9 shows the ultimate state of the physical hybrid model and lateral load–displacement relations from the experimental and FE models of the hybrid model, respectively. For the physical and numerical results, the nonlinear load–displacement curves of T2 had more ductile and less stiff slope changes than those of T1. As the lateral displacement increased, the resistance gradually increased and converged to 1.1 kN; the resistance was greater than 1.9 times that of T1. According to the identical yield point estimation to T1 for T2, the yield resistance was estimated to be 0.8 kN. The subsidence of the soil surface in the

opposite side of the monopile loading direction occurred while a smaller soil heaving of the surface in the side of the loading direction than T1 was observed.

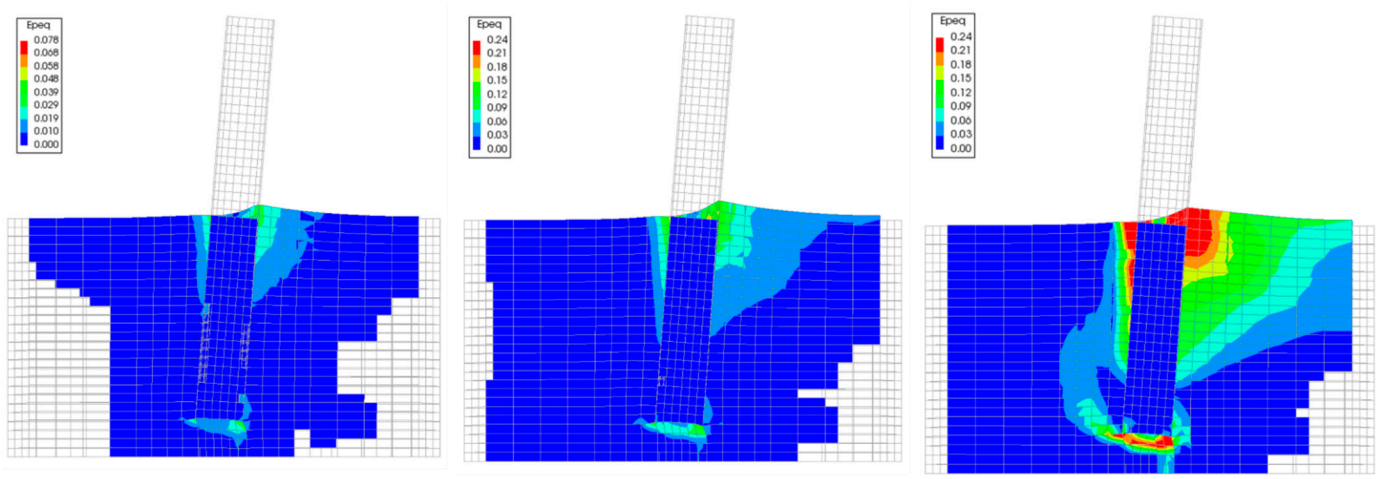

(**a**) (**b**) (**c**)

Figure 8. Failure of monopile foundation: (**a**) initial loading ($\delta = 5$ mm); (**b**) peak load ($\delta = 30$ mm); (**c**) residual state ($\delta = 80$ mm); where δ: lateral displacement at the top of the monopile, Epeq: equivalent plastic strain (mm/mm).

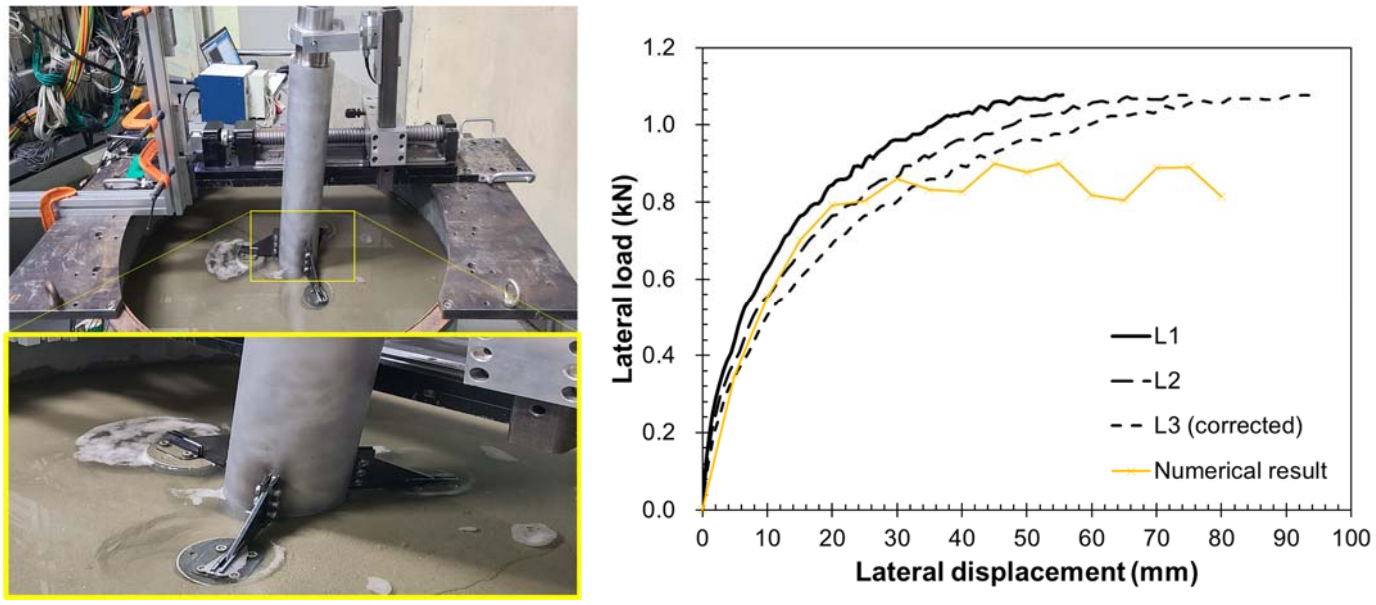

(**a**) (**b**)

Figure 9. Physical and FE-based test comparison for hybrid monopile: (**a**) surface subsidence after loading of physical test; (**b**) load–displacement curves from physical and FE models.

In other hands, the numerical resistance of T2 agreed with those of the physical test until the lateral displacement of 10 mm, and the slope rapidly decrease after 20 mm. The peak resistance 0.90 kN occurred at 45 mm and then the resistance decreased gradually; the numerical model underestimates the T2 resistance to 82%.

Figure 10 shows the equivalent plastic strain changes to visualize the soil failure mechanism for the hybrid monopile. A soil plastic deformation not only occurred at T1 but also near the bucket skirt and tip. In initial lateral loading, the soil in the compression around both the wall and tip of the monopile became plastic, and the soil in the tension behind the pull-outing bucket as well. Unlike T1, which had a plastic area limited to the

near monopile, the buckets distributed an external load even far from the soil around the monopile and caused wider soil failure zones; this contributed to the hybrid monopile being able to resist a lateral force.

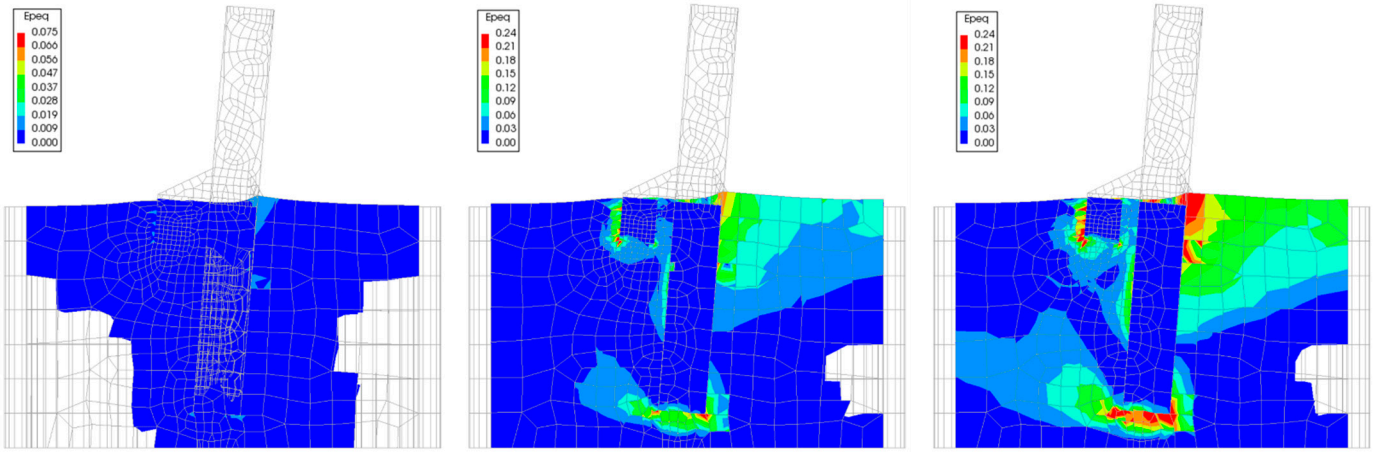

(**a**) (**b**) (**c**)

Figure 10. Failure of hybrid monopile foundation: (**a**) initial loading (δ = 5 mm); (**b**) peak load (δ = 45 mm); (**c**) residual state (δ = 80 mm); where δ: lateral displacement at the top of the monopile, Epeq: equivalent plastic strain (mm/mm).

3.3. Comparison with Results

Changes in the behaviors of the monopile due to the supplemental support were also investigated numerically. Figure 11 shows the distributions of normal stresses in the direction of z and the lateral displacement in the external loading direction along the monopiles. The numerical data were extracted from the nodes on the back of the monopile with respect to the loading direction to compare the result distributions with minimizing the disturbance of the adjacent other structural members such as the wing plate.

As shown in Figure 11, the monopiles rotated like a rigid body regardless of the magnitude of the maximum lateral displacement at the top and differences between the curves did not appear. In other hands, the stress distributions of the monopiles were slightly different. For applying the displacement load, for the normal stress in the z-direction, although the curves were similar to each other, the monopile with the supplemental support had a greater lateral resistance than that of the monopile only. The result can be explained by the enlargement of the soil resistance area and a change in the soil bearing mechanism due to the installation of the bucket type of a supplemental support, as follows. With respect to the monopile, the soil and supplemental support play a role as the constraint to prevent the deformation and displacement of the monopile and the constraints cause the increased stresses of the monopile. The lateral movements of only a monopile installation cannot be constrained after the soil around the monopile reached the ultimate state while the hybrid monopile movement is restricted by wider soil due to the supplemental support and itself; this means a more external load is required for the soil to be perfectly plastic. The supplemental support also assists to distribute the external loads which have been supported by the monopile only, and leads to the transfer of the lateral soil bearing to the vertical; these help the hybrid monopile to be able to resist external loads more.

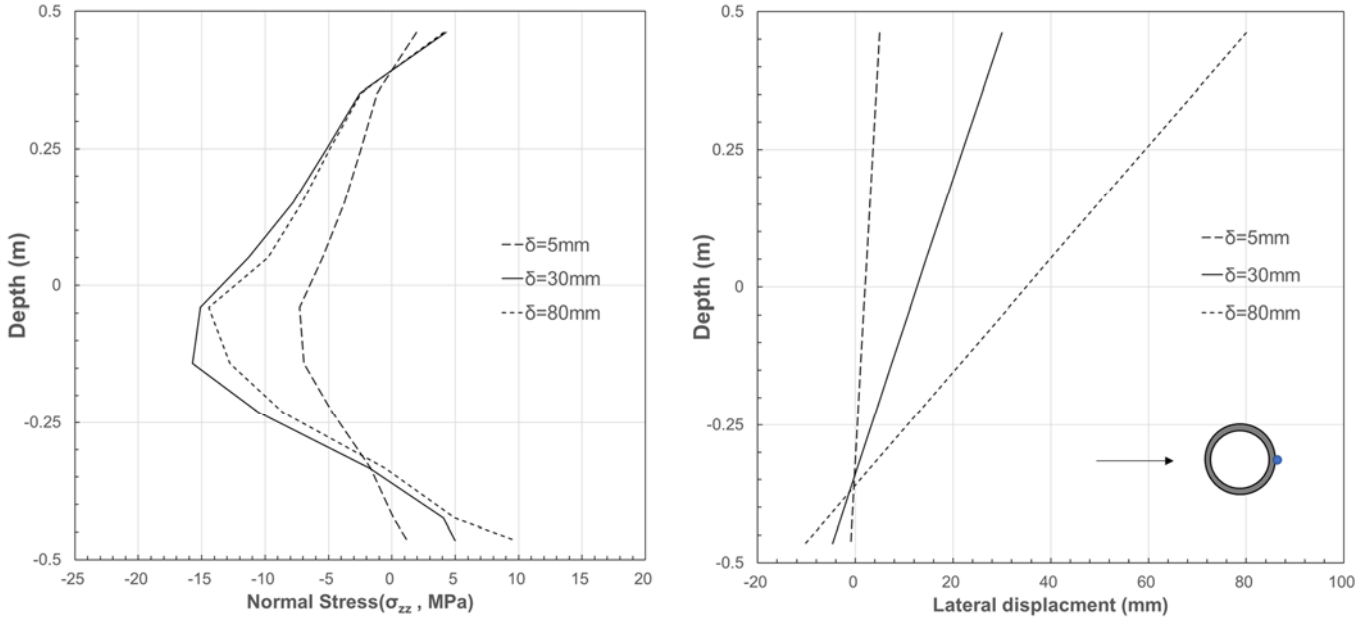

(**a**)

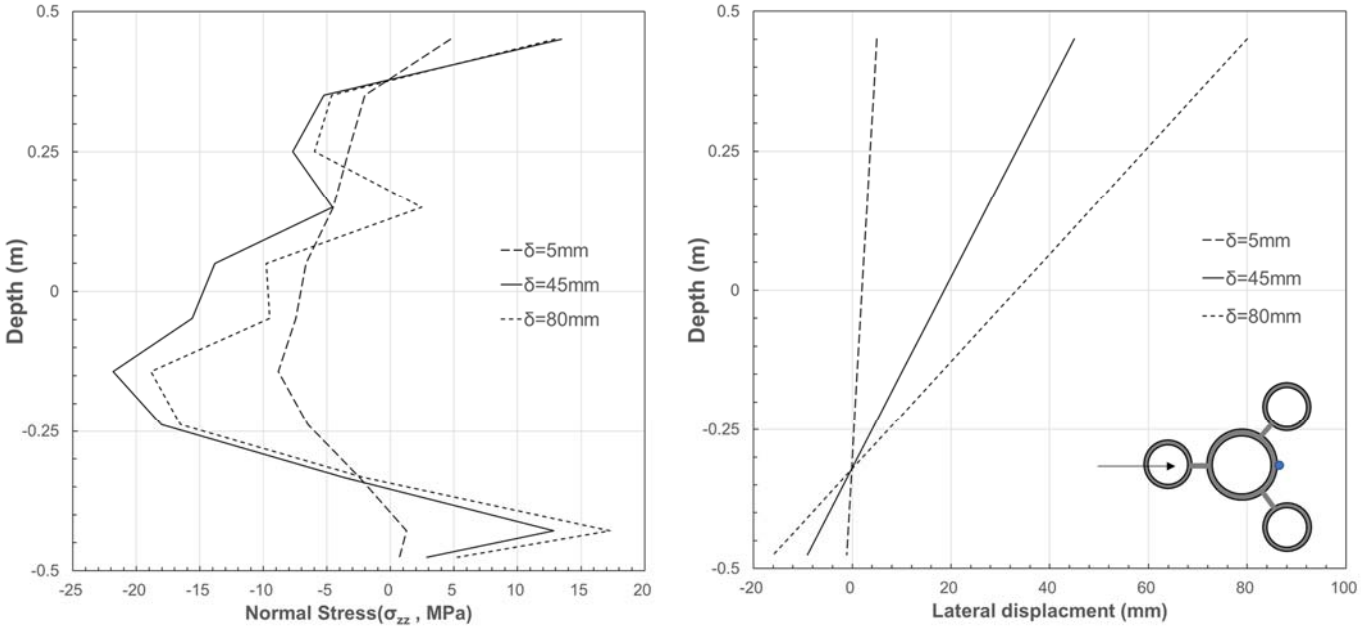

(**b**)

Figure 11. Normal stress (σ_{zz}) and lateral displacement distribution profiles along monopiles: (**a**) monopile; (**b**) hybrid monopile; where each diagram on lower right corner of (**a**,**b**) indicates a cross-section of the conventional and the hybrid monopiles, respectively; black arrow: load direction, blue point: observation location.

4. Case Study of Hybrid Monopile for 5.5 MW OWT Installed in Korean Seabed

4.1. Environmental Site Characteristics

The case studies of the 5.5 MW OWT hybrid monopile support (Figure 1) installed at a representative Korean weak soil area were conducted using FE analysis. As shown in Figure 12, two sites which were considered as one of the Korean wind energy farm candidates were selected; though these are not the worst seabed conditions, the sites represent the area and have a proper soil layer composition to observe the effect of the

hybrid monopile. Case A is deeply distributed weak sand and its average water depth is 20 m, while Case B has several types of weak soil layers and a weathered rock bed to 27 m from the seabed surface. From the geotechnical investigation reports of the sites, the main specific soil layer descriptions are summarized in Table 5. For each site, although the offshore condition is different, assuming a water depth of 20 m and a 50 return period, the identical wave condition was applied due to the limitation in obtaining the ultimate load data: a maximum wave height of 11.94 m, a wave period of 11.16 s, a wave length of 139.39 m, and a current velocity of 1.396 m/s were obtained.

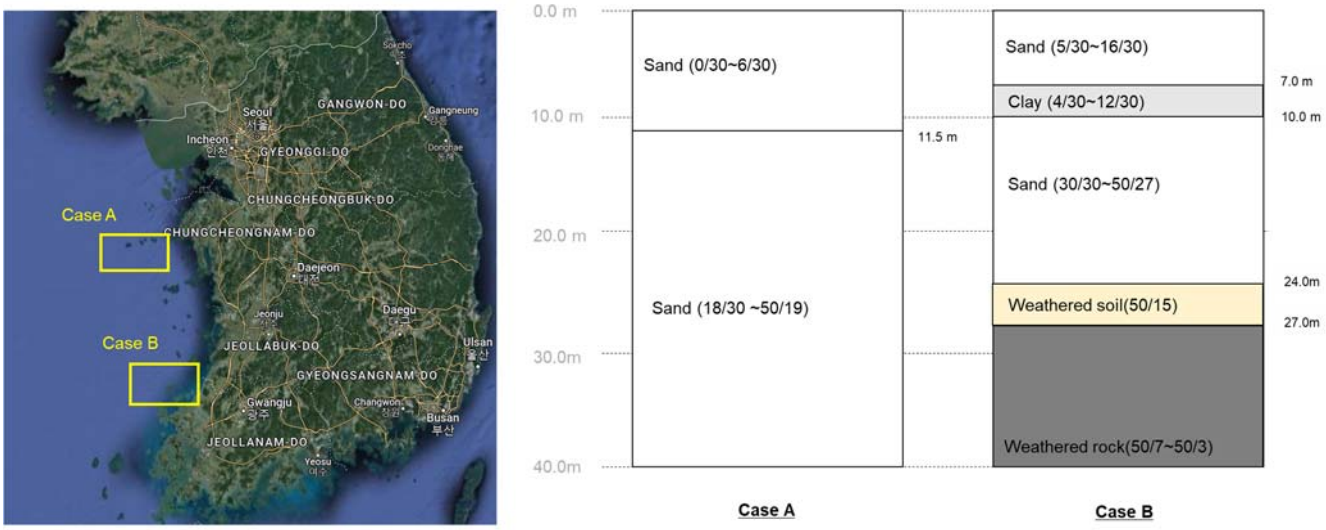

Figure 12. Target sites and its soil layer composition.

Table 5. Soil layer and input parameters *.

Case	Layer	Depth (m)	ρ_{sub} (kg/m^3)	c (kPa)	ϕ (°)	E (kPa)
A	Sand	0.0~11.5	770.00	0.1	20.37	4350.00
	Sand	11.5~56.5	815.56	0.1	43.44	57,468.25
B	Sand	0.0~7.0	917.43	0.1	27.0	24,249
	Clay	7.0~10.0	867.48	44.6	0.0	4852
	Sand	10.0~24.0	917.43	0.1	38.0	47,476
	Weathered soil	24.0~27.0	1019.37	30.0	44.5	55,750
	Weathered rock	27.0~	1223.24	30.0	49.5	67,200

* ρ_{sub}: submerged density; c: cohesion; ϕ: internal friction angle; E: elastic modulus.

4.2. Model Descriptions

Three-dimensional finite element models of the hybrid foundation for both cases A and B were generated using DIANA FEA. The main dimensions of the models are as shown in Figures 1 and 13. the dimensions were determined considering the soils bearing capacities of the suction buckets; the lengths of the bucket skirt for cases A and B were 5.9 m and 5.4 m, respectively. In the finite element models, the shell elements were used to model most structure members except the grout between the monopile and casing, while the solid elements were used for the soil and grout region. To analyze the numerical behaviors of the hybrid monopile, the corresponding monopile model was also created.

Because the complex behaviors of the pile-casing connection were expected due to shear keys, the part was simplified that the monopile and casing are perfectly bonded using grout; this approach can facilitate a clear understanding of the soil–structure interaction changes in the hybrid monopile. It was assumed that the monopile and the supplemental support made with S355 behaves according to the von Mises plasticity, while soil responses were described using MC plasticity.

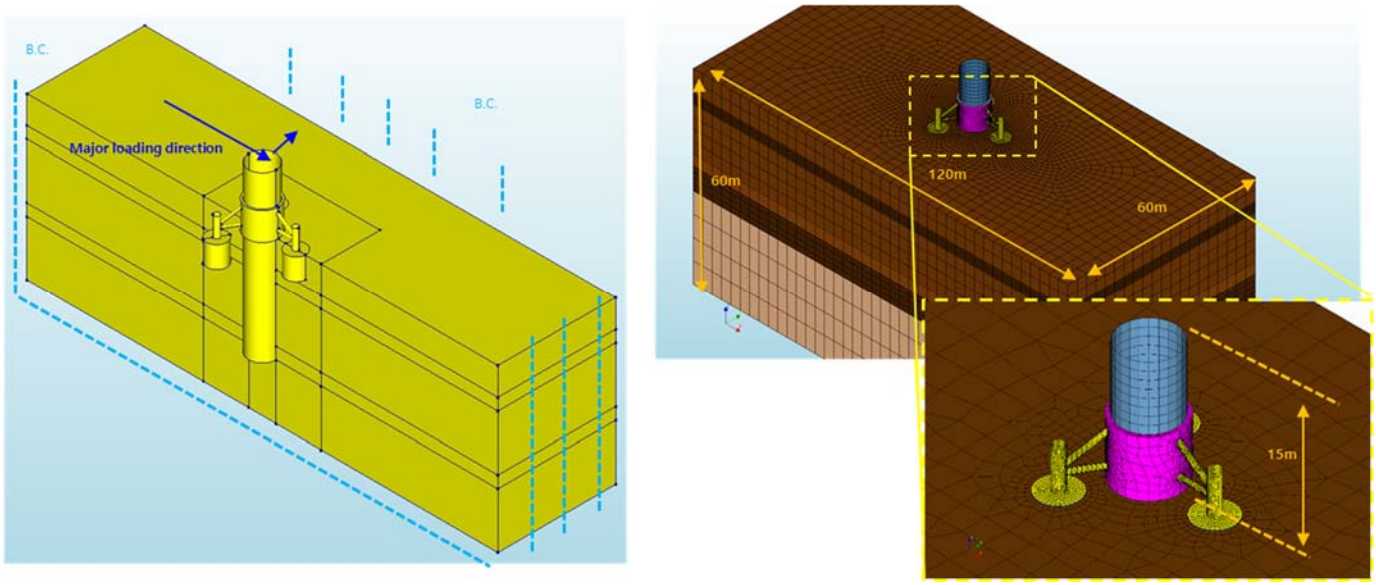

(**a**) (**b**)

Figure 13. Model geometry and mesh (Case B): (**a**) load and boundary conditions (**b**) finite element mesh; where B.C.: boundary conditions.

The model was simplified as a representation of the partial area of the OWT substructure to reduce the computational time and to consider the functions of the adopted tools. Unfortunately, the offshore load calculation is not provided in DIANA FEA. For this reason, the external forces have been estimated using a frame element model, generated in ANSYS ASAS which supports several wave load functions. For the monopile supporting of a wind turbine of the 5.5 MW OWT, the load components were extracted from the corresponding location (15 m higher than the seabed surface) on the frame model in which the loading point of the solid-shell combination model was matched within. To reproduce the more realistic behaviors of the hybrid monopile, construction stage analyses were conducted for cases A and B: geostatic state analysis, physical model installation, and lateral loading.

Among the design load conditions (DLCs), the DLC 4.2 case, as representative critical load conditions, was adapted to the model. By following the above procedure, the external load was calculated including the OWT load at the transition piece and a wave condition with the current. The calculated load components in the finite element model for the case study are summarized in Table 6; the indicated components were applied to the models with a safety factor of 1.35. To apply the load components at the top of the monopile in the models, a tying point was set on the top edge of the monopile to prevent from a stress concentration near the loading point due to the concentrated load.

Table 6. Load components of DLC 4.2 for cases A and B.

F_x (MN)	F_y (MN)	F_z (MN)	M_x (MN·m)	M_y (MN·m)	M_z (MN·m)
5.764	−0.013	−0.993	5.691	140.940	0.648

The vertical and horizontal displacement constraints were imposed to the soil boundaries to be zero in the normal direction of the boundary surfaces. The allowed interface elements, but no tension, were applied at the contact surfaces between the soil and structures, such as in Section 3.

4.3. Results

4.3.1. Case A

Figure 14 shows the numerical results of both the monopile only and hybrid monopile for case A. The lateral displacements of the monopile were greater than that of the hybrid

while the effect on the soil due to the structure area was smaller. However, because the weak soil layer with low strength and stiffness properties spreads, the supplemental support was not able to distribute the internal forces of the monopile into itself and soil. Although the displacement at the seabed surface slightly decreased for the hybrid monopile, the difference was little: just 14 mm.

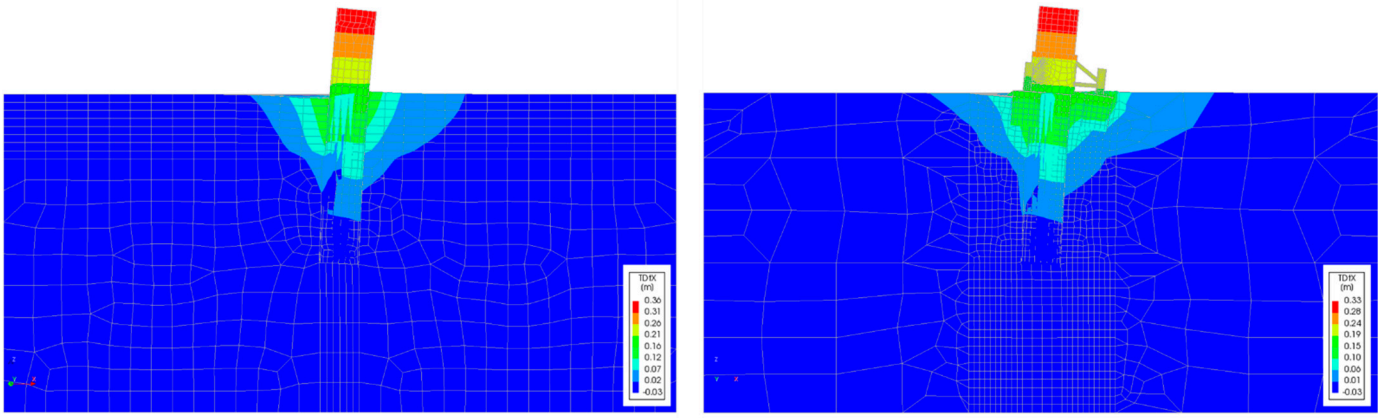

(**a**)

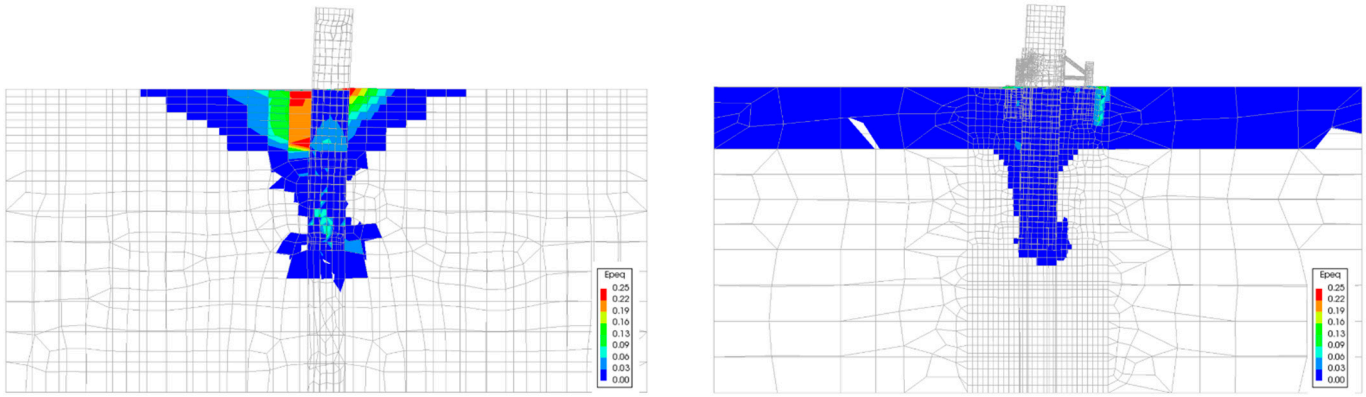

(**b**)

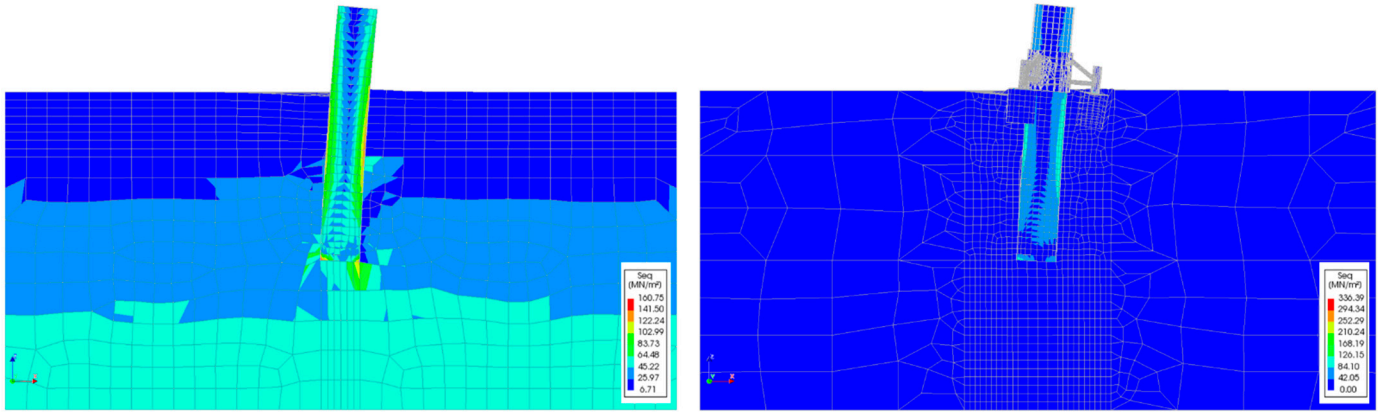

(**c**)

Figure 14. Comparison with results of monopile and hybrid monopile for case A: (**a**) lateral displacement; (**b**) equivalent plastic strain; (**c**) von Mises equivalent stress.

Plastic deformations of soil in the upper layers near the structures widely occurred for the hybrid monopile compared with those of the monopile only case; the plastic strains for the latter case were relatively evenly and widely spread along the depth. The plastic

deformation distribution also supported the tri-buckets which failed to play a role as a supplemental support for case A.

The stresses of the hybrid monopile excess to the yield strength were found. The excessive stresses occurred at the lid adjacent to the vertical pipe and at the edge between the lid and the skirt of the bucket that was aligned in the same direction of the loading. For the diagonal and horizontal pipes connected to the vertical pipe, the stresses at the ends much increased.

4.3.2. Case B

Although case B has weak soil layers, the contributions of the supplemental support to the improvement of the lateral behaviors of a monopile were remarkable (Figure 15). In regard to the seabed surface, the lateral displacement of the monopile decreased to 72.7% of that of the monopile only case. The top soil layer of case B has a greater elastic modulus and internal friction angle than those of case A. This would make the supplemental support bring out the vertical bearing capacity as well as the lateral.

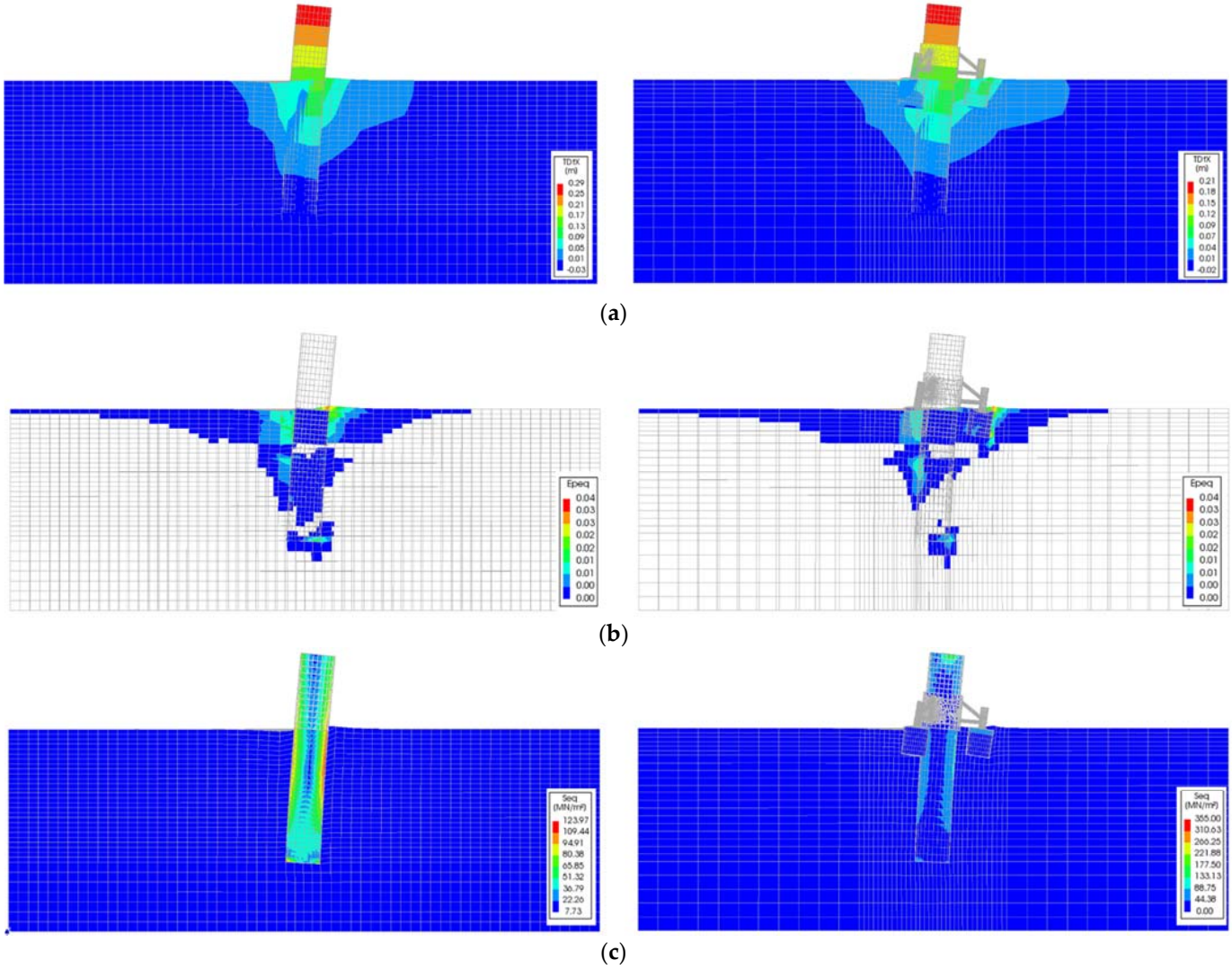

Figure 15. Comparison with results of monopile and hybrid monopile for case B: (**a**) lateral displacement; (**b**) equivalent plastic strain; (**c**) von Mises equivalent stress.

The plastic deformations distributions of the hybrid monopile were similar to that of the monopile only; the main difference in the distributions was that more plastic deformations occurred near the seabed concentratedly for the hybrid monopile. The plastic

deformations along the depth were wider in the monopile only case and consequently would become failed soon, while the soil bearing capacities of the hybrid monopile remains.

The stresses of the hybrid monopile also yielded to the yield strength like case A. The excessive stresses occurred at the same positions with case A. This means the supplemental support requires more stiffeners to reduce the stresses and displacement of the suction buckets.

4.3.3. Summary and Comparison with Results of Cases A and B

The results of the case studies related to the main design factors of the monopile foundation design are listed in Table 7. The remarkable contribution of the supplemental support to decreasing both the displacement and rotation of the monopile at the seabed's surface is shown for case B only, while that of case A is not shown. Thus, the application of the supplemental support obviously helps to reduce the lateral displacement in the case of the enough vertical bearing capacity of the soil.

Table 7. Result comparison with cases A and B.

Case		δ_{seabed} (m)	θ_{seabed} (°)	$\sigma_{max,MP}$ (MPa)	$\sigma_{max,Supp.}$ (MPa)
A	Monopile	0.194	0.413	161.0	-
	Hybrid monopile	0.180	0.401	149.0	355.0
B	Monopile	0.145	0.370	124.0	-
	Hybrid monopile	0.104	0.224	150.0	355.0

In other hands, the structural members adjacent to and composed of the suction bucket in the compression are yielded. Referring to the practical examples and studies related to the suction bucket with a diameter of 5 m and above, many radial stiffeners were attached to the lid to prevent the bending of the bucket. The lid of the suction bucket in this study has no reinforcement, although a large vertical external force transfers to the lid, considering the structural shape of the supplemental support.

5. Discussion

5.1. Scale Effects of Small-Scaled Model Tests

When an experiment is performed with a small-scaled model to simulate the real structural behavior under the field condition, the scale effects need to be carefully considered due to the stress discrepancy between the actual and the laboratory soil. This section discusses the scale effects on the results of the physical model tests which affect the behavior of a small-scaled monopile foundation.

According to previous studies [27–30] on the physical model test of the soil, the effects of the soil particle size on the current physical model tests are minimal when the ratio between the mean soil particle size (D_{50}) and structure is greater than 60. In this study, the mean diameter of the GS soil particle and the diameter of the small-scaled models for the monopile are D_{50} = 0.08 mm and D = 109.62 mm (outer diameter), respectively; the ratio is D_{50}/D = 1370. Thus, the particle size effect is negligible for the current study.

The main purpose of the small-scaled model test is to investigate the lateral displacement changes due to the proposed supplementary support. Although a geometrical similarity between the small-scaled and real models was maintained in this study, similar soil conditions including a confining stress and material stiffness were limited to be reproduced because model tests were conducted in a 1g environment. Conventionally, the field soil experiences a higher confining stress level as the soil depth is deeper, while the soil in the small-scaled 1g tests is under a low confining stress. Additionally, the dense soil tends to be dilated under the high confining stress, whereas the contractive behavior is governed under the low confining stress. These behavioral characteristics hinder the extrapolation of the results from the scaled model tests into the field. Such a difference in the soil behavior depending on a confining stress level can be overcome by carrying out the model test in a

loose soil where the compressive behaviors are shown regardless of the confining stress. For this reason, the present study conducted model tests in loose soil so that the differences in the soil behavior between the field and the model were minimized. However, in this study, a similarity for flexural rigidity, such as the pile thickness and material stiffness, were not considered due to the difficulty of manufacturing the small monopile. Namely, the small-scaled model tests were performed for a very rigid monopile compared with that of the field cases, so that the results of this study have to be understood as the case limited to specific experimental conditions.

5.2. Comparitive Analysis with Other Types of Hybrid Monopiles

There are several restrictions when comparing with the behaviors of each hybrid monopile systems because of the different conditions of the loading method, scale size, soil conditions, etc. Nevertheless, a comparison with the effects of the supplemental supports on each monopile behavior could be valuable.

For the collared monopile, Jepsen and Kristiansen [20] designed the diameter of each collar and monopile as 14 m and 4.5 m considering mass optimization and the stress safety requirement. However, because they modeled the collared monopile to be simplified for soil modeling as fixed boundary conditions, the contribution of the collar to reducing the lateral displacement of the monopile at the seabed and to increasing the bearing capacity of the hybrid system cannot be estimated. On the other hand, Arshi's research team [5,21] analyzed the bearing capacities of the hybrid monopile system with the collar by a small physical push over the tests under a 1 g condition. The ultimate lateral resistance of the hybrid monopile in cohesionless soil increased up to 50% and 100% compared with that of the monopile as increasing the diameter of the supplemental support. Although their studies verified several important design factors of the hybrid monopile by physical tests, the scale size of the models were not given. Thus, their results are also difficult to directly compare with those of the present study.

Furthermore, Yang's research team [17] conducted finite element analyses and centrifuge model tests of the hybrid monopile with a mono-bucket for cohesionless soil; the hybrid monopile is called as pile-bucket foundation by them. They conducted push-over tests under a 50 g condition and the test models were built with a similarity ratio of 50 for the Putian project [16]. Using the similarity ratio, the diameter and the embedding length of the monopile are estimated to be 6.5 m and 30 m, respectively. For the mono-bucket, the diameter and the skirt length are 26 m and 6 m. According to the results from the experiments and finite element analyses, the ultimate lateral bearing capacity of the hybrid increased up to about 100~129% compared with that of the monopile. For the present hybrid monopile of this study, the increasing ratio of the ultimate resistance of the hybrid to the conventional monopiles is 90%. Comparing with the dimensions of each model, the monopile diameter is similar with each other, while the supplemental support of the proposed hybrid model is much smaller than the pile-bucket foundation; the area ratio of the large mono-bucket to the tri-bucket is 0.17. However, it is not reasonable to directly compare with the ultimate bearing capacities because a push-over test under a 1 g condition cannot reproduce identical soil stress states to those of the field as well as the material similarity. For the discussion, it is necessary for each hybrid system to be set more under similar conditions.

6. Conclusions

This paper proposed a hybrid monopile with a tri-bucket supplemental support and then analyzed the behaviors of the proposed hybrid system by small-scaled model tests as well as validating via an FE simulation. The applicability of the proposed hybrid system was also comprehensively evaluated to potentially use as an OWT foundation in the two local Korean offshore sites using the FE model.

From the small-scaled model tests, it was shown that the proposed hybrid system contributes to reducing the rotation of the monopile and increasing the lateral resistance

up to 90% compared with that of the conventional monopile. The proposed supplemental support also makes the lateral behaviors of the monopile foundation ductile, which is furthermore confirmed via an FE simulation investigation. Namely, the ductile behaviors of the foundation are explained to be caused by both the extension and redistribution of the soil resistance area due to the supplemental support.

Finally, the proposed hybrid monopile of a full scale are numerically simulated under two different Korean seabed conditions to investigate the more realistic behaviors of the hybrid monopile. The proposed hybrid system shows that the tri-bucket type of the supplemental support reduces the lateral displacement and effectively distributes the internal forces of the monopile to soil that has enough vertical bearing capacities. Particularly for the hybrid system of case B, the lateral translational and rotational displacements at the seabed surface decrease down to 73% and 61% of those of the conventional monopile, respectively. Although the proposed supplemental support requires reinforcements and/or shape changes to decrease the stress concentration of the buckets in future, it is clarified that the supplemental support can be an efficient alternative to overcome excessive tilting or lateral displacement at the seabed, and to satisfy the serviceability design of the OWTs monopile foundation.

The ultimate bearing capacities of the previous hybrid monopile system and their conditions were discussed to evaluate the proposed hybrid monopile and advantages. The finding of the comparison with the ultimate resistance of each hybrid system is that the proposed hybrid system is evaluated, effectively increasing the resistance compared to that of the monopile despite the small area of the supplemental support. However, it is hard to claim that the proposed hybrid monopile is more effective than the others because of differences in the load test condition, especially for the soil stress state. Thus, future studies should aim to real the scale model test or small-scaled centrifuge tests of the proposed hybrid monopile. Additionally, the applicability of the proposed monopile has to be validated by physical tests under various conditions: the soil types, soil composition, and structure dimensions.

Author Contributions: J.K. coordinated the writing of the paper and conducted the FE analyses. Y.-J.J. proposed the conceptual shape of the new monopile and investigated prior similar studies. J.P. contributed to estimate the soil properties in the FE analysis and examined the numerical result validation. J.-H.L. and T.K. designed and conducted the physical model tests. J.-H.K. supported the physical model tests and provided the fundamental soil parameters by laboratory tests. All authors have read and agreed to the published version of the manuscript.

Funding: This research was supported by the Korean Institute of Energy Technology Evaluation and Planning (KETEP) and grant funded by the Korea government (MOTIE) (No.20208520130010, Development of hybrid monopile technology based on frictional resistance for offshore wind turbine).

Institutional Review Board Statement: Not applicable.

Informed Consent Statement: Not applicable.

Data Availability Statement: The data are not publicly available due to confidential constraints. The data presented in this study are partially available on request from the corresponding author after all the collaborator's approval.

Acknowledgments: The authors would like to acknowledge all the collaboration and support provided by offshore structure engineering provider Zentech and Geotechnical engineering provider GeoOcean.

Conflicts of Interest: The authors declare no conflict of interest.

References

1. Accelerating Offshore Wind through Partnerships. Available online: https://www.cowi.com/insights/accelerating-offshore-wind-through-partnerships (accessed on 23 August 2022).
2. Wang, X.; Zeng, X.; Yang, X.; Li, J. Feasibility study of offshore wind turbines with hybrid monopile foundation based on centrifuge modeling. *Appl. Energy* **2018**, *209*, 127–137. [CrossRef]

3. Jeong, Y.J.; Park, M.S.; Kim, J.; Song, S.H. Wave force characteristics of large-sized offshore wind support structures to sea levels and wave conditions. *Appl. Sci.* **2019**, *9*, 1855. [CrossRef]
4. El-Marassi, M. Investigation of Hybrid Monopile-Footing Foundation System Subjected to Combined Loading. Ph.D. Thesis, The University of Western Ontario, London, ON, Canada, 6 September 2011.
5. Arshi, H.S.; Stone, K.J.L.; Vaziri, M.; Newson, T.A.; El-Marassi, M.; Taylor, R.N.; Goodey, R.J. Modelling of monopile-footing foundation system for offshore structures in cohesionless soils. In Proceedings of the 18th International Conference on Soil Mechanics and Geotechnical Engineering, Paris, France, 2–6 September 2013.
6. Anastasopoulos, I.; Theofilou, M. Hybrid foundation for offshore wind turbines: Environmental and seismic loading. *Soil Dyn. Earthq. Eng.* **2016**, *80*, 192–209. [CrossRef]
7. Anderson, M.C. The Hybrid Monopile: Design of A Novel Foundation Structure for Large Offshore Wind Turbines in Intermediate Water Depths. Master Thesis, Delft University of Technology, Delft, The Netherlands, 9 August 2017.
8. Yang, X.; Zeng, X.; Wang, X.; Li, X. Assessment of monopile-gravel wheel foundations under lateral-moment loading for offshore wind turbines. *J. Waterw. Port Coast. Ocean Eng.* **2019**, *145*, 04018034. [CrossRef]
9. Ma, H.; Yang, J. A novel hybrid monopile foundation for offshore wind turbines. *Ocean Eng.* **2020**, *198*, 106963. [CrossRef]
10. Huang, Y.; Han, X. Features of earthquake-induced seabed liquefaction and mitigation strategies of novel marine structures. *J. Mar. Sci. Eng.* **2020**, *8*, 310. [CrossRef]
11. Cho, Y.J. Scour controlling effect of hybrid mono-pile as a substructure of offshore wind turbine: A numerical study. *Mar. Sci. Eng.* **2020**, *8*, 637. [CrossRef]
12. Li, X.; Zeng, X.; Wang, X. Feasibility study of monopile-friction wheel bucket hybrid foundation for offshore wind turbine. *Ocean Eng.* **2020**, *204*, 107276. [CrossRef]
13. Wang, X.; Li, J. Parametric study of hybrid monopile foundation for offshore wind turbines in cohesionless soil. *Ocean Eng.* **2020**, *218*, 108172. [CrossRef]
14. Trojnar, K. Simplified design of new hybrid monopile foundations for offshore wind turbines. *Ocean Eng.* **2021**, *219*, 108046. [CrossRef]
15. Li, Y.; Shi, W.; Li, X.; Wang, B. Analysis of the dynamic characteristics of the top flange pile driving process of a novel monopile foundation without a transition section. *Sustainability* **2022**, *14*, 5950. [CrossRef]
16. First Monopile-Caisson Hybrid Foundation Installed at Chinese Offshore Wind Farm. Available online: https://www.offshore-energy.biz/first-monopile-caisson-hybrid-foundation-installed-at-chinese-offshore-wind-farm/ (accessed on 23 August 2022).
17. Wang, J.; Sun, G.; Chen, G.; Yang, X. Finite element analyses of improved lateral performance of monopile when combined with bucket foundation for offshore wind turbines. *Appl. Ocean Res.* **2021**, *111*, 102647. [CrossRef]
18. RWE to Deploy Collared Monopiles at Kaskasi Offshore Wind Farm. Available online: https://www.offshorewind.biz/2020/11/30/rwe-to-deploy-collared-monopiles-at-kaskasi-offshore-wind-farm/ (accessed on 23 August 2022).
19. Collared Monopile Debuts on RWE's Kaskasi Offshore Wind Farm. Available online: https://www.offshorewind.biz/2022/06/08/collared-monopile-debuts-on-rwes-kaskasi-offshore-wind-farm/ (accessed on 23 August 2022).
20. Arshi, H.S.; Stone, K.J.L. Lateral resistance of hybrid monopile-footing foundations in cohesionless soils for offshore wind turbine. In Proceedings of the 7th International Conference on Offshore Site Investigation and Geotechnics, London, UK, 2–6 September 2012.
21. Jepsen, M.; Kristiansen, J. *A Hybrid Foundation for Offshore Wind Turbines: Analysis of A Collared Monopile Foundation*; SDA8-1-F21; Aalborg University: Aalborg, Denmark, 2021.
22. Kim, J.; Jeong, Y.J.; Park, M.S.; Song, S.H. Structural behavior analysis of offshore wind support structure with monopile considering pile-soil interaction. *J. Wind Energy* **2020**, *11*, 38–47. (In Korean)
23. DNVGL. *DNV-ST-0126: Support Structure for Wind Turbines*; Det Norske Veritas: Oslo, Norway, 2018.
24. Smith, I.M.; Griffiths, D.V. *Programming the Finite Element Method*, 4th ed.; John Wiley & Sons: Hoboken, NJ, USA, 2004.
25. Kim, J.H. Model Testing Foundations for Offshore Structure in the Centrifuge and Development of Miniature Cone. Ph.D. Thesis, KAIST, Daejeon, Republic of Korea, 31 August 2016.
26. Vilalobos, F.A. Model Testing of Foundations for Offshore Wind Turbines. Ph.D. Thesis, University of Oxford, Oxford, UK, 2006.
27. Ovesen, N.K. Panel discussion in session 9: The use of physical models in design. In Proceedings of the 7th European Conference on Soil Mechanics and Foundation Engineering, British Geotechnical Society, Brighton, UK, 10–13 September 1979; Volume 4, pp. 319–323.
28. Franke, E.; Muth, G. Scale effect in 1-g model tests on horizontally loaded piles. In Proceedings of the 11th International Conference on Soil Mechanics and Foundation Engineering, San Francisco, CA, USA, 12–16 August 1985; Volume 2, pp. 1011–1014.
29. Sedran, G.; Stolle, D.F.E.; Horvath, R.G. An investigation of scaling and dimensional analysis of axially loaded piles. *Can. Geotech. J.* **2001**, *38*, 530–541. [CrossRef]
30. Verdure, L.; Garnier, J.; Levacher, D. Lateral cyclic loading of single piles in sand. *Int. J. Phys. Modell. Geotech.* **2003**, *3*, 17–28. [CrossRef]